Draft, to be published as a LHC-B technical note and as a ROSE technical note

Analysis of the Radiation Tolerance of the LHC-B Silicon Vertex Detector

H. Feick
ROSE/CERN - RD48 Collaboration

II. Institut für Experimentalphysik, Universität Hamburg,
Luruper Chaussee 149, 22761 Hamburg, Germany

Abstract

This note analyses the radiation tolerance of the LHC-B silicon vertex detector in the framework of the latest damage models put forward by the ROSE / CERN RD 48 Collaboration. The calculations assume constant temperature and constant flux for a one year beam period of 240 d. It is found that the ultimate failure of the detectors is due to the damage-induced doping changes causing the loss of sensitive volume. Increases in the leakage current and carrier trapping stay at a tolerable level. Given a suitable operating temperature (5°C) and initial resistivity, detectors of 150 µm (480 Ωcm) and 200 µm (850 Ωcm) thickness are expected to remain fully depleted with 200 V up to equivalent 1-MeV neutron fluences of 5×10^{14} cm^{-2} and 9×10^{14} cm^{-2}, respectively. Admitting partially depleted operation, the lower benchmark figure of 7000 collected electrons is reached at radiation doses as high as 8×10^{14} cm^{-2} and 1×10^{15} cm^{-2}, respectively. A conservative 50% error in the quoted values is due to the uncertainty in the experimentally determined constants of the damage models.

Analysis of the Radiation Tolerance of the LHC-B Silicon Vertex Detector

H. Feick
ROSE / CERN - RD48 Collaboration

II. Institut für Experimentalphysik, Universität Hamburg,
Luruper Chaussee 149, 22761 Hamburg, Germany

Abstract

This note analyses the radiation tolerance of the LHC-B silicon vertex detector in the framework of the latest damage models put forward by the ROSE / CERN RD 48 Collaboration. The calculations assume constant temperature and constant flux for a one year beam period of 240 d. It is found that the ultimate failure of the detectors is due to the damage-induced doping changes causing the loss of sensitive volume. Increases in the leakage current and carrier trapping stay at a tolerable level. Given a suitable operating temperature (5°C) and initial resistivity, detectors of 150 µm (480 Ωcm) and 200 µm (850 Ωcm) thickness are expected to remain fully depleted with 200 V up to equivalent 1-MeV neutron fluences of 5×10^{14} cm^{-2} and 9×10^{14} cm^{-2}, respectively. Admitting partially depleted operation, the lower benchmark figure of 7000 collected electrons is reached at radiation doses as high as 8×10^{14} cm^{-2} and 1×10^{15} cm^{-2}, respectively. A conservative 50% error in the quoted values is due to the uncertainty in the experimentally determined constants of the damage models.

1. Introduction

The LHC-B experiment will be running at a luminosity of 2×10^{32} $cm^{-2}s^{-1}$ resulting in an annual equivalent 1-MeV neutron fluence of about 1×10^{14} cm^{-2} at the innermost radius (1 cm) of the silicon vertex detector [1]. For safety reasons it is also worthwhile considering higher doses as additional radiation might be generated, e.g. by a lost beam. It is well known that at such radiation levels a serious deterioration of the silicon detectors must be envisaged, see e.g. [2]. The LHC-B Collaboration has well recognized this situation and gave a first estimate of the tracker performance degradation in ref. [3]. In this note we give a detailed description of the damage-induced changes in the doping concentration, leakage current, and charge collection based on the expertise of the ROSE Collaboration [4]. In particular we will highlight the implications of the material used for the manufacture of the detectors and the temperature maintained during their operation. At this point we also include our latest findings reported in ref. [5]. Still it was necessary to further refine the models as a) freezing of the beneficial annealing in the doping changes and b) charge collection at arbitrary fields had so far not been treated in enough detail, however, these issues turn out to be important for LHC-B. These and other more technical aspects are detailed in the Appendix. The bulk of the paper consists of the application of the damage models to the particular operating conditions met at LHC-B (Sect. 3.), the presentation of the results (Sect. 4.), and the discussion of the errors and weaknesses in the approach used (Sect. 5.).

2. Detector Parameters and Operational Conditions

A parameter of paramount importance for the operation of silicon detectors is the full depletion voltage V_{dep}. For our purposes it is sufficient to approximate V_{dep} by the expression

$$V_{dep} = |N_{eff}| \, d^2 \, q_0 \, / 2 \, \varepsilon \, \varepsilon_0 . \qquad (1)$$

It is evident that even for large absolute values of the effective doping concentration $|N_{eff}|$ (e.g. brought about by radiation damage) a reasonably low V_{dep} can be obtained if the detector thickness d is made sufficiently small. In this report we consider either d = 200 µm, which is a quite optimistic figure for a wafer to be processed with standard equipment, or d = 150 µm, clearly being a challenge for the detector supplier due to the resulting mechanical instability. A small thickness also aids reducing the radiation length, however, it compromises the number of electron-hole pairs generated in the detector by a traversing particle. Detectors are assumed to be manufactured on comparatively low resistivity n-type silicon, suitable to counteract the damage-induced negative space charge [5]. As the operational voltage V_{op} is assumed in this note to be fixed to 200 V, we specified an initial depletion voltage V_{dep0} of 150 V for either thickness. The corresponding initial doping concentration N_{eff0}, compare eq. (1), and initial resistivity $\rho \approx (q_0 \, \mu_n N_{eff0})^{-1}$ is listed in Table 1. Initial leakage currents are regarded as negligible compared with the damage-induced bulk generation current. For purpose of clarity all currents in this note are given normalized to area. In order to determine the current in a particular channel, the actual segmentation of the LHC-B vertex detectors has to be taken into account which is left to the interested reader.

d	V_{dep0}	N_{eff0}	ρ (20°C)[a)]
150 µm	150 V	8.8×10^{12} cm^{-3}	480 Ωcm
200 µm	150 V	4.9×10^{12} cm^{-3}	850 Ωcm

[a)] using μ_n = 1480 cm²/Vs

Table 1. The two alternative sets of detector parameters studied.

The analysis given in the following sections assumes a t_{exp} = 240 d lasting operation at a constant average particle flux $\phi_{eq} = F_{eq} \, / \, t_{exp}$. F_{eq} denotes the equivalent 1-MeV neutron fluence absorbed in that time. Also the operating temperature T_{op} is assumed to be a constant. Results will be presented for values of F_{eq} and T_{op} ranging between 2…8×10^{14} cm^{-2} and -10…25°C, respectively.

3. Modeling Bulk Damage Effects at LHC-B

In this section the equations describing the macroscopic damage effects for constant flux and constant temperature operation are just written down without derivation from the basics. For a more detailed introduction into the physics behind the damage models see for example [6].

Doping Changes

In general the damage-induced change in the doping concentration $\Delta N_{eff} = N_{eff0} - N_{eff}$ can be split into three parts

$$\Delta N_{eff} = N_a + N_c + N_Y . \qquad (2)$$

They account for the fractions exhibiting short term (beneficial) annealing (N_a), no annealing (N_c), and long term (reverse and/or anti) annealing (N_Y). Here we will presuppose that the first component can be visualized as to arise from a single acceptor introduced per volume at the rate $g_a \, \Phi_{eq}$ and decaying at the rate k_a, for details see Appendix A. The solution of the appropriate differential equation under the given operational conditions writes

$$N_a (t) = g_a \, \Phi_{eq} \, [1 - \exp(- k_a \, t)] / k_a , \qquad (3)$$

where t is the time elapsed since the beam was switched on. As the stable damage component N_c does not exhibit annealing it is only implicitly depending on time via the accumulated fluence $\Phi_{eq} \, t$:

$$N_c \, (t) = N_{c0} (1 - \exp(- c \, \Phi_{eq} \, t)) + g_c \, \Phi_{eq} \, t . \qquad (4)$$

Again, an acceptor introduced with the damage rate g_c can be thought of to be the origin of the term on the right-hand side of eq. (4). Conversely, the term on the left-hand side is considered to be due to the removal of donors at the rate $c \, \Phi_{eq}$. In fact, for fluences greater than $3 / c \approx 10^{13}$ cm^{-2} these donors with initial concentration N_{c0} are almost completely exhausted. In this context the following relation was found by systemic studies on various detector materials with different resistivity [6]

$$N_{c0} = 0.3 \times N_{eff0} + 0.1 \times 10^{12} \text{ cm}^{-3}, \qquad (5)$$

That is, N_{c0} is notably smaller than the phosphorus concentration of the original material[†]. Eq. (5) is of particular importance as it points to a reservoir of non-removable donors with concentration $\approx 0.7 \times N_{eff0}$ causing the higher radiation tolerance of lower resistivity material.

An other result reported in ref. [5] concerns the reverse annealing component N_Y. It was found that the corresponding microscopic process is essentially of 1st order while 2nd order kinetics had been assumed so far. In order to account for this circumstance, the following expression has been used in this work (compare eq. (3))

$$N_Y (t) = g_Y \, \Phi_{eq} \, t - g_Y \, \Phi_{eq} \, [1 - \exp(- k_{Y1} \, t)] / k_{Y1} . \qquad (6)$$

The reasoning for this approach and the relation between the 2nd order and 1st order annealing rates is left for Appendix C.

While the doping concentration is not considered to be temperature dependent by itself, both the beneficial annealing (k_a) and the reverse annealing (k_{Y1}) rates obey the Arrhenius-relation

$$k = k_0 \exp(- E_a / k_B T). \qquad (7)$$

[†] Here the compensation of the original material with boron has been assumed to be very low. This was actually proven by photo luminescence spectroscopy [7]. Therefore N_{eff0} is almost entirely due to donors.

Frequency factors k_0 and activation energies E_a are characteristic of the specific annealing process in question and need to be established experimentally, see Appendix A and C.

Leakage Current

The damage-induced increase in the leakage current I per area A has been calculated with

$$\frac{I}{A}(t,T) = W\alpha_\infty R^{-1}(T)\sum_{i=0}\frac{a_i}{a_0}f_{eq}\tau_i(T)\left[1-\exp\left(-t/\tau_i(T)\right)\right]. \tag{8}$$

W denotes the width of the depleted region

$$W = d \times \min\left((V_{op}/V_{dep})^{1/2}, 1 \right). \tag{9}$$

Thus, the loss of active volume occurring in partial depletion operation is taken into account. $\alpha_¥$ is the current related damage constant as it is observed at room temperature (T_R = 20°C) after complete annealing‡.

Intrinsically the leakage current originating from damage-induced bulk generation centers varies strongly with temperature. This is accounted for by the dimensionless scaling factor

$$R(T) = \left(T_R/T\right)^2 \exp\left(-\frac{E_g}{2k_B}\left[\frac{1}{T_R}-\frac{1}{T}\right]\right). \tag{10}$$

Here E_g is an empirical parameter related to the effective energetic position of a single deep level representing the sum of all current generation centers introduced by bulk damage. E_g has a value of about the band gap of the semiconductor.

Steady-state introduction and annealing of the generation centers is treated similar to the beneficial annealing of the doping concentration, see eq. (3). However, as the leakage current annealing curve has originally been parameterized by a sum of exponential terms $a_i \exp(-t/\tau_i)$, each has been identified here with an independent defect requiring the summation made in eq. (8). In this note the parameters listed in Table 2 have been used. They describe the normalized annealing function at room temperature for inverted detectors.

i	0	1	2	3	4
$\tau_i(T_R)$ **[d]**	∞	6.07	1.08	5.9×10^{-2}	9.4×10^{-3}
a_i	0.243	0.139	0.121	0.300	0.197

Table 2. Parameterization of the normalized leakage current annealing curve (room temperature) for inverted detectors, from [9].

‡ Meanwhile it is known that on detectors operated with reasonable protection against edge leakage (e.g. grounded guard ring) the annealing process is not observed to come to rest at all [8]. More detailed studies on this subject are underway.

The decrease of the annealing rate at low temperature can be accounted for by scaling the time constants measured at room temperature [6]: $\tau_i(T) = \tau_i(T_R) / \varphi(T)$. Only a single activation energy is thereby assumed to characterize the annealing at the microscopic level. Thus, the scaling factor is

$$\varphi(T) = \exp\left(\frac{E_I}{k_B}\left[\frac{1}{T_R} - \frac{1}{T}\right]\right), \tag{11}$$

as can be inferred from the general Arrhenius-relation eq. (7).

Charge Collection

$$\tau_{tr,n}^{-1}(F_{eq}) = \tau_{tr,n0}^{-1} + \begin{cases} g_n F_{eq} & F_{eq} < F_{eq}^* \\ g_n^*(F_{eq} - F_{eq}^*) + g_n F_{eq}^* & F_{eq} > F_{eq}^* \end{cases} \tag{12}$$
$$\tau_{tr,p}^{-1}(F_{eq}) = \tau_{tr,p0}^{-1} + g_p F_{eq}$$

Inversion fluence F_{eq}* see eq. (A.4) in Appendix B.

Tmax = 25 ns

Damage Parameters

Doping Concentration	
g_a	1.54×10^{-2} cm^{-1}
k_{0a}	2.3×10^{13} s^{-1}
E_{aa}	1.08 eV
c	2.29×10^{-13} cm²
g_c	1.77×10^{-2} cm^{-1}
g_Y	4.60×10^{-2} cm^{-1}
k_{0Y1}	8.74×10^{14} s^{-1}
E_{aY}	1.31 eV

Leakage Current	
α	2.86×10^{-17} A/cm
E_I	1.09 eV
E_g	1.24 eV

Charge Collection	
$\tau_{tr,n0} = \tau_{tr,p0}$	1.96 µs
$g_n = g_p$	0.24 cm²/µs
g_n*	1.01 cm²/µs

Table 3. Numerical values of the damage parameters used for the calculations. If not revised in this note, the values are the global data compiled for neutron damage in ref. [2].

4. Results

$F_{eq}(R) = F_{eq}(1\ \text{cm}) / R^2$

$T_{op}(R) = 3°\text{C/cm}\ (R - 1\ \text{cm}) + 5°\text{C}$

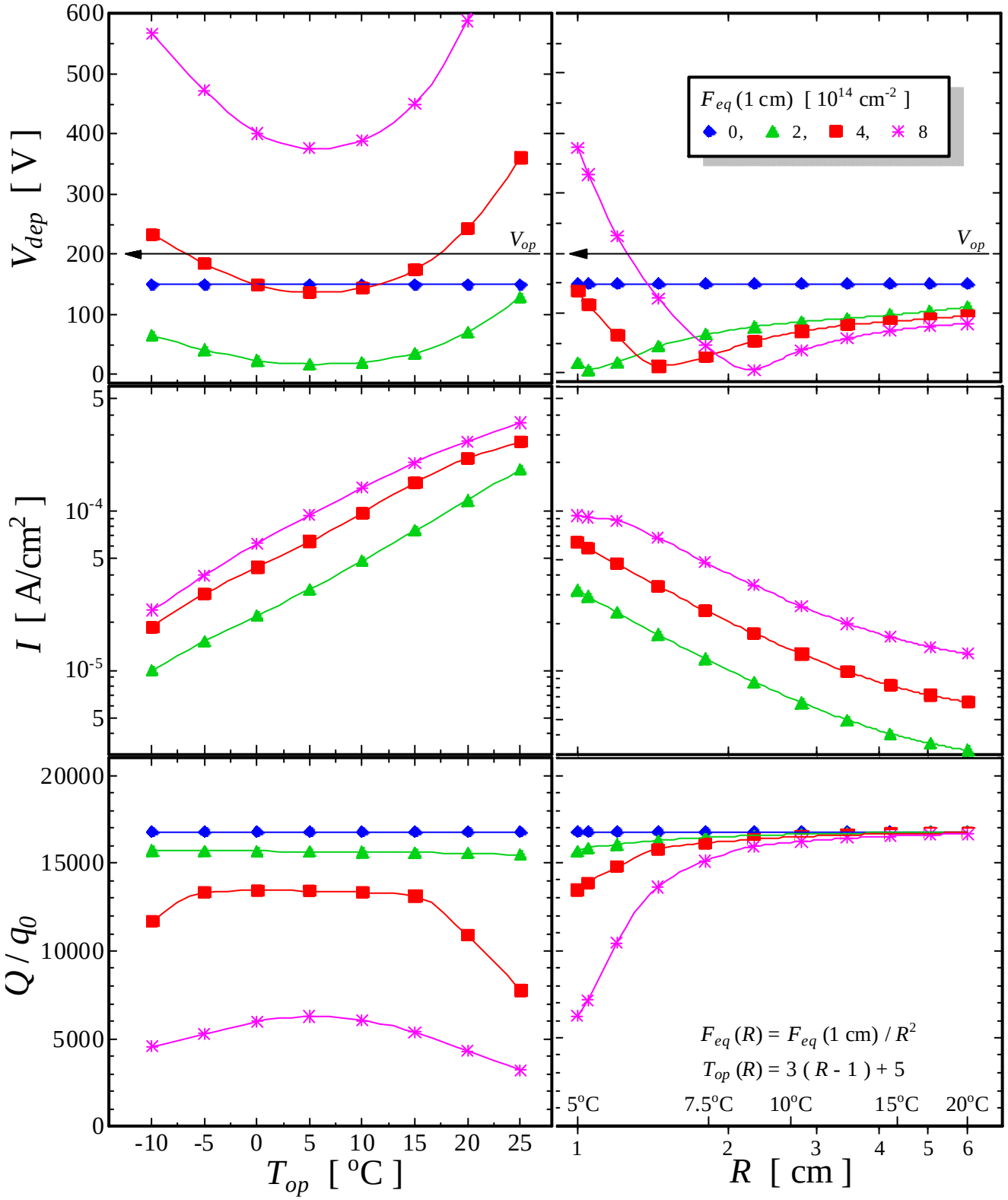

Fig. 1. Results for d = 200 µm

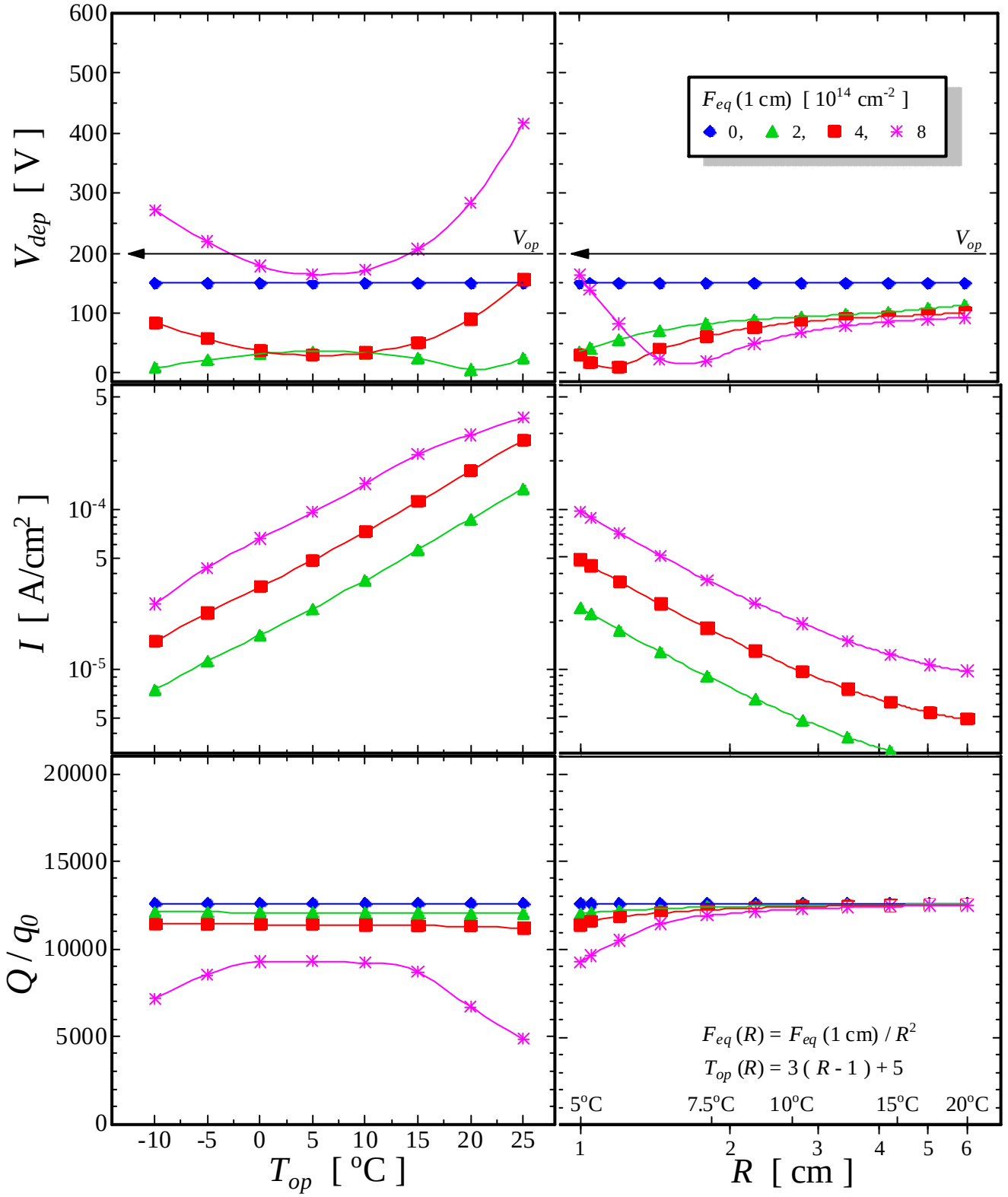

Fig. 2. Results for d = 150 µm

5. Discussion

Operating Temperature

T	-10	-5	0	5	10	15	20	25
t_a [d]	2.43×10^{2}	1.00×10^{2}	4.25×10^{1}	1.86×10^{1}	8.40×10^{0}	3.90×10^{0}	1.86×10^{0}	9.07×10^{-1}
t_{Y1} [d]	1.62×10^{5}	5.53×10^{4}	1.96×10^{4}	7.20×10^{3}	2.74×10^{3}	1.08×10^{3}	4.40×10^{2}	1.84×10^{2}
R	20.3	11.8	6.95	4.17	2.55	1.59	1.00	0.641
q	7.31×10^{-3}	1.79×10^{-2}	4.25×10^{-2}	9.76×10^{-2}	2.18×10^{-1}	4.73×10^{-1}	1.00×10^{0}	2.06×10^{0}

Table 4. Parameters deciding on the choice of the optimum operating temperature.

Starting Material

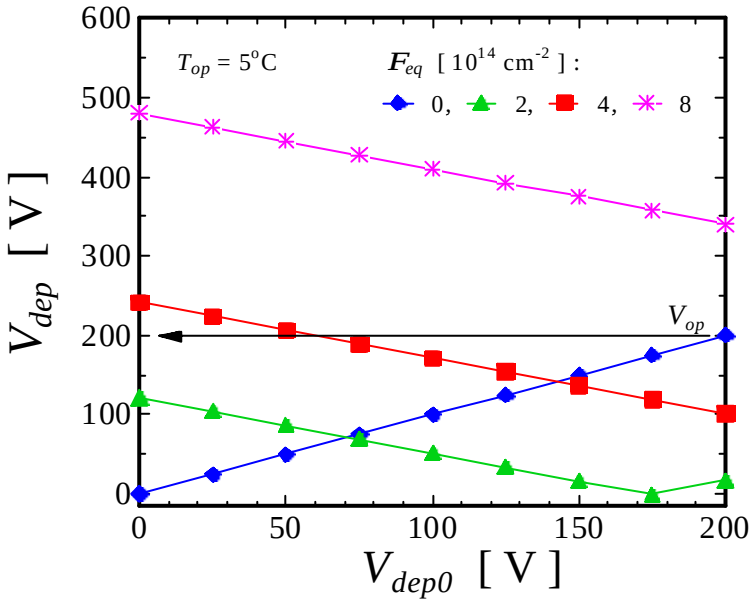

Fig. 3. Variation of the final depletion voltage with the initial depletion voltage for d = 200 µm.

Accuracy

Acknowledgements

Financial support is acknowledged to the Hamburg Group from the BMBF under contract 05 7HH 17 I. Discussions with Hans Dijkstra, Gunnar Lindström, and Eckhart Fretwurst are greatly appreciated.

Appendix A: Beneficial Annealing of the Doping Concentration

The variation of the full depletion voltage observed directly after a short term exposure to heavy-particle irradiation is attributed to the annealing of a small number of acceptors. This approach corresponds to a mathematical representation of the annealing curve by a sum of exponential terms $a_i \exp(-t/t_i)$. As annealing time constants of the order of minutes or hours are not relevant to the operation of silicon detectors in high-energy physics experiments, only the longest decay time constant t_a will be considered here. For a specific irradiation with 1 MeV-neutron-equivalent fluence F_{eq} the contribution from this portion to the overall doping change varies with time as

$$N_a(t) = g_a F_{eq} \exp(-t/t_a). \qquad (A.1)$$

In this note t_a-data have been compiled from literature along with the corresponding introduction rates g_a, see Table A.1.

T [°C]	t_a [d]	g_a [10^{-2} cm^{-1}]	k	Reference
-10	440±32[a]			[10]
0	44±2.0	1.26±0.02	0.582[b]	[11] M40
0	66.7±4.8[a]			[10]
10	8.3±0.7	1.68±0.05	0.582[b]	[11] M44
10	12.1±0.87[a]			[10]
10	5.8±1.0	1.45±0.28	2.89[c]	[12] Mean pC
10	4.6±1.1	1.05±0.03	0.94[d]	[12] Mean πC
20	2.0±0.32	2.23±0.17	0.582[b]	[11] M18
21	1.8±0.13[a]	1.78	≈ 1.10[e]	[10]
25	1.5±0.5	0.69±0.37	0.94[d]	[12] Mean πW
60	(1.45±0.09)×10^{-2}	2.2±0.2	1.44[f]	[13]

[a] Error taken as the difference between the data points and the fit in [10]
[b] Experimental value (ref. [6]) for the 24 GeV/c p at CERN PS
[c] 21 MeV p at MPI Heidelberg
[d] 190 MeV π+ at PSI
[e] 647 MeV and/or 800 MeV p at LAMPF
[f] <5.3> MeV n at PTB Be(d,n)

Table A.1. Annealing time constant and introduction rate as function of temperature compiled from literature.

The annealing time constant is the inverse of the corresponding annealing rate. Thus, according to the Arrhenius-relation eq. (8), it is

$$t_a^{-1} = k_a = k_{0a} \exp(-E_{aa}/k_B T). \qquad (A.2)$$

Fig. A.1. demonstrates the reasonable agreement between the experimental values and eq. (A.2). It will be noted that the individual errors in the t_a data quoted in Table A.1 were not used as weights because the resulting χ^2 was much larger than the number of degrees-of-freedom of the problem. These errors must therefore be considered unreliable and cannot be used as they might lead to a wrong fit. Consequently, a common unknown error has been estimated from the straight-line fit. The numerical results are

$$E_{aa} = (1.08 \pm 0.05) \text{ eV}$$
$$k_{0a} = 2.3^{18}_{0.29} \times 10^{13} \text{ s}^{-1}.$$

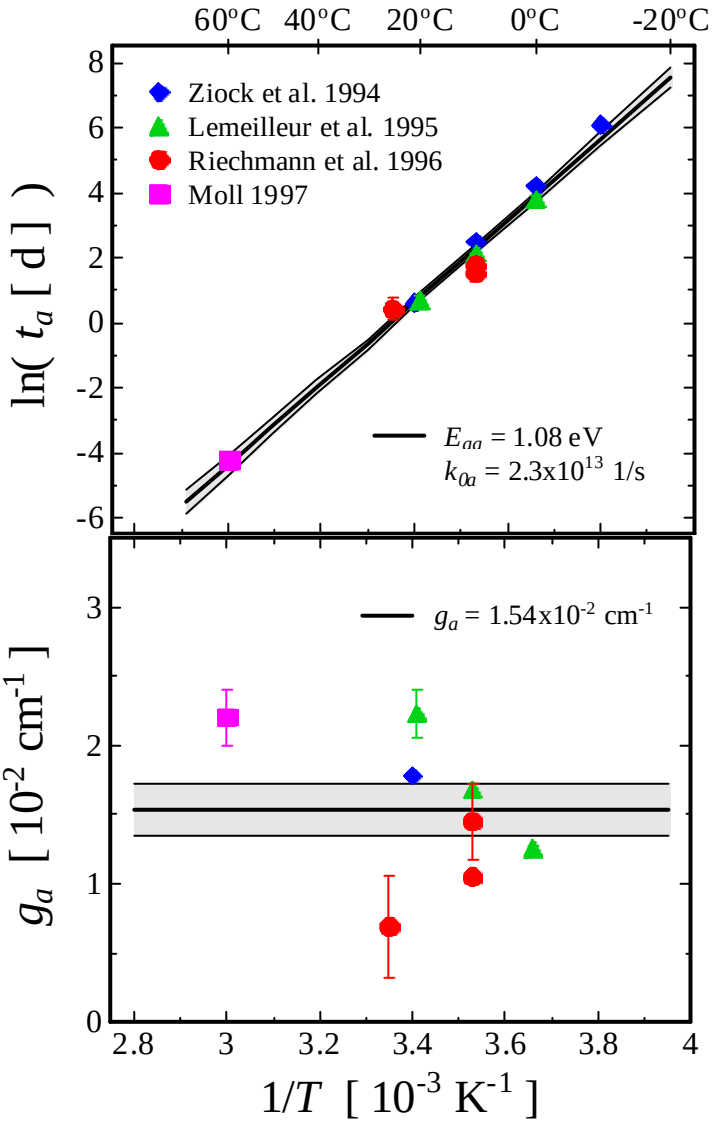

Fig. A.1 Top: Arrhenius plot for the longest annealing time constant. Bottom: corresponding introduction rates. The shaded area represents the prognosis error in the fitted quantity.

It is worth noting the approximately equal values of the activation energies characteristic of the short term annealing of the doping concentration E_{aa} and the leakage current E_1, see Table 2. This provides evidence for a

similar origin of the two phenomena, as was already concluded earlier by means of a correlation of the overall annealing curves [14]. Here we have in addition gained the frequency factor k_{0a} which in the temperature range studied is of the order of the most abundant phonon frequency $k_B T / h \approx 10^{13}$ s^{-1}. At the microscopic level the annealing processes do therefore require only a single jump (dissociation or reorientation) rather than long range migration.

Introduction rates g_a have been normalized to equivalent 1 MeV-neutron values using the hardness factor k quoted in Table A.1. For mono-energetic sources with particle energy E_p it is

$$k = D(E_p) / 95 \text{ MeVmb.} \qquad \text{(A.3)}$$

$D(E_p)$ denotes the displacement damage cross section and/or damage function. With this definition the 1 MeV-neutron-fluence equivalent to the fluence F is given by $F_{eq} = k F$. If not stated otherwise, the numerical evaluations of $D(E_p)$ as recommended by the ROSE Collaboration have been used here [5]. Further details on the calculation of k, also for wide spectrum sources, can for example be found in ref. [15]. Due to the reasons already mentioned above the individual errors in g_a listed in Table A.1 have not been taken into account. The non-weighted average of the normalized introduction rates and the corresponding error is then found to be (compare Fig. A.1 bottom)

$$g_a = (1.54 \pm 0.19) \times 10^{-2} \text{ cm}^{-1}$$

There is clearly a significant spread around the average value originating from systematic errors. Their sources are various, as for example i) the method used for the evaluation of CV curves, ii) the procedure used for the fitting of the annealing function, iii) the source calibration, and so on. Also the influence of the starting material, a potential hidden parameter in the evaluation, has not yet been thoroughly investigated.

Appendix B: The Inversion Fluence

As an application of eq. (5) we can very grossly determine the inversion fluence F_{eq}* at which the sign of the space charge changes from positive to negative, that is, where N_{eff} equals zero. It will be assumed that the corresponding change in the doping concentration $DN_{eff} = N_{eff0} - N_{eff} = N_{eff0}$ is due only to the stable damage component N_c. This ensures inversion even if the annealing and the reverse annealing fraction are at a certain time much smaller than N_c. Moreover, it will be anticipated that for conventional materials F_{eq}* is so large that all donors with concentration N_{c0} are removed. Then eq. (4) reduces to $N_c \approx N_{c0} + g_c F_{eq}$* and substitution of eq. (5) yields

$$F_{eq}^* \approx (N_{eff0} - N_{c0}) / g_c \approx 40 \text{ cm} \times N_{eff0}. \qquad \text{(A.4)}$$

In view of the above presuppositions it is obvious that eq. (6) gives an upper limit of the inversion fluence. For the instance of a short term exposure not allowing for beneficial annealing, g_c must be replaced with $g_c + g_a$. This gives $F_{eq}^* \approx 21 \text{ cm} \times N_{eff0}$, which is in good agreement with the result obtained in ref. [16].

Appendix C: Reverse Annealing — a Process of Effectively 1st Order

Reverse annealing data as measured on a silicon detector in the long term after a short term exposure to bulk damaging radiation is best parameterized by the function

$$N_Y(t) = g_Y F_{eq} [\, 1 - (1 + g_Y F_{eq} k_Y t \,)^{-1} \,]. \qquad \text{(A.5)}$$

Originally it was believed that two neutral defects of equal concentrations combine to form an acceptor by a 2nd order reaction. Recently it was found that the 2nd order rate constant k_Y in eq. (A.4) varies with fluence as $1 / F_{eq}$ [6]. This does then however point to 1st order kinetics at the microscopic level. While therefore the use of eq. (A.4) in conjunction with a fluence dependent rate constant $k_Y(F_{eq})$ is still valuable for the description of laboratory annealing data, it is not straight-forward to derive a model valid during steady-state irradiation as required for high-energy physics applications. In order to circumvent these difficulties it will be noted that eq. (A.4) is equal to

$$N_Y(t) = g_Y F_{eq} [\, 1 - \exp(- g_Y F_{eq} k_Y t \,) \,] \qquad \text{(A.6)}$$

as long as $g_Y F_{eq} k_Y t$ is much smaller than unity. Indeed, the reverse annealing time constant is about one year at room temperature and much larger at lower temperature. Thus, under the operational conditions anticipated at LHC experiments the used approach is well justified. Evidently the equivalent 1st order annealing time constant is given by

$$k_{Y1} = g_Y F_{eq} k_Y(F_{eq}) = 1.9 \times 10^{16} \text{ cm/s} \times g_Y \exp(- E_{aY} / k_B T), \qquad \text{(A.6)}$$

where $k_Y(F_{eq})$ has been substituted with the empirical expression found in [6]. Moreover, identifying eq. (A.6) with the Arrhenius-relation eq. (8) gives the corresponding frequency factor $k_{0Y1} = 1.9 \times 10^{16}$ cm/s $\times g_Y$. As eq. (A.5) is the solution of a usual differential equation of 1st order it is now easy to include an inhomogeneity accounting for the steady-state generation of neutral defects transforming into acceptors during reverse annealing. The solution is given by eq. (7).

References

[1] H. Dijkstra, private communication.

[2] A. Chilingarov et al. „Radiation studies and operational projections for silicon in the ATLAS inner detector“ Nucl. Instr. and Meth. A 360 (1995) 432-437.

[3] O. Cooke „The effect of radiation damage on the vertex detector efficiency“ LHCB 97-023 TRACKING (December 1997)

[4] The ROSE collaboration, CERN/LHCC 96-23 (1996).

[5] The ROSE collaboration, first status report to the LHCC, CERN/LHCC 97-39 (July 1997), ftp://ftp.brunel.ac.uk/ph/phsf/rose/ROSE-status-report.ps.

[6] H. Feick „Radiation Tolerance of Silicon Particle Detectors for High-Energy Physics Experiments“ Ph.D. thesis Universität Hamburg, Internal Report DESY F35D-97-08 (1997)

[7] B.C. MacEvoy „Defect Kinetics in Silicon Detector Material for Applications at the Large Hadron Collider“ Ph.D. thesis, Imperial College London, RAL-TH-97-003 (1997)

[8] E. Fretwurst et al. „A comprehensive model for the behavior of irradiated silicon detectors“ presented at the Third International (Hiroshima) Symposium on the Development and Application of Semiconductor Tracking Detectors at Melbourne 9-12th , December, 1997, to be published in Nucl. Instr. and Meth.
[9] R. Wunstorf „Systematische Untersuchungen zur Strahlenresistenz von Silizium-Detektoren für die Verwendung in Hochenergiephysik-Experimenten“ Ph.D. thesis, Universität Hamburg, DESY FH1K-92-01 (1992)
[10] H.-J. Ziock et al., Nucl. Instr. and Meth. A 342 (1994) 96-104.
[11] F. Lemeilleur et al., Nucl. Instr. and Meth. A 360 (1995) 438-444.
[12] K. Riechmann et al., Nucl. Instr. and Meth. A 377 (1996) 276-283.
[13] M. Moll, private communication.
[14] J. Matheson et al. „A microscopic explanation for type inversion and the annealing behaviour of radiation damaged silicon detectors“ Nucl. Instr. and Meth. A 371 (1996) 575-577
[15] A. Vasilescu „Overview of the radiation environment in ATLAS and CMS SCT and the irradiation facilities used for damage tests : excerpt from thesis“ ROSE/TN/97-3, http://www.brunel.ac.uk/research/rose/ps/rosetn973.ps
[16] S.J. Bates et al. „Proton irradiation of silicon detectors with different resistivities“ CERN/ECP 95-18.